EFFECT OF AXIAL LOAD ON TORSION FATIGUE BEHAVIOR OF WOOD

Mariko Yamasaki

Research Associate
Graduate School of Engineering
Nagoya Institute of Technology
Gokiso-cho, Showa-ku, 466-8555 Nagoya, Japan

and

Yasutoshi Sasaki

Professor
Graduate School of Bioagricultural Sciences
Nagoya University
Furo-cho, Chikusa-ku, 464-8601 Nagoya, Japan

(Received August 2007)

ABSTRACT

The torsion fatigue behavior of solid wood under cyclic torsion-axial combined loading was investigated. The test specimens used were air-dried Japanese cypress that were cut into sections of 17.5 mm (tangential) × 17.5 mm (radial), with their major axis lying along the fiber direction of 300 mm (longitudinal). A pulsating torsion with a triangular waveform was applied along the longitudinal axis of the specimens at 1 Hz, while the specimen was also simultaneously subjected to an axial (tension or compression) load at the same phase along the longitudinal direction, at stress levels corresponding to 50–100% of each static strength. The results obtained are summarized as follows: When tension was added to pure torsion, the inclination of the *S-N* curve tended to decrease as the tensile stress component increased. On the other hand, when compression was added to pure torsion, the *S-N* curve generally moved to the long-life side. The strength of the wood was different between dynamic and static modes, under not only pure loading but also axial-torsion combined loading. The torsion deformation under compression-torsion combined loading kept its initial value small until the increase before final failure, and this was considered to cause the lengthening of the fatigue life under the stress state, in which shear and compression stress components were almost equal.

Keywords: Fatigue, combined loading, compression, tension, torsion.

INTRODUCTION

The fatigue behavior of wood under combined axial and shear stresses is considered. In this study, we focus on the torsion fatigue of wood and consider the effect of the axial force (tension or compression) exerted on the torsion fatigue characteristics. Previous studies that can be considered as background for this work are introduced as follows. Okuyama et al. (1984) conducted an experimental study on the compression and tension fatigue of solid wood. The fatigue fracture of wood was discussed on the basis of time-dependent fractures. The material used in their experiments was air-dried spruce (*Picea* sp.). A pulsating sine load was applied to specimens for the tension and compression tests at both 0.1 and 10 Hz along the longitudinal axis of the specimens, which coincided with the fiber direction of the wood. According to their results, the cyclic number to failure in compression was larger than that in tension, and a longer time for fracturing was required for the higher frequency when the stress levels were the same. A comparison between fatigue fracture and static fracture based on the time for fracturing showed that tensile fatigue fracture occurred in a shorter period of time than static fracture, whereas the compressive fatigue failure took a longer time

than the static failure. That is, their *S-N* lines showed that the fatigue life of wood was lengthened as a result of cyclic compressive loading.

On the other hand, Ando et al. (2005) investigated the torsion fatigue properties of two wood species (Japanese beech and white cedar) under controlled torque. Pulsating torsion with a reversed sine waveform and loading frequencies of either 0.1 or 1 Hz was applied along the longitudinal direction of the wood. Their results showed that a negative linear relationship can be observed between the shear stress level and the number of cycles to failure (N_f, fatigue life) on the semilogarithmic graph, and that the N_f at the frequency of 1 Hz was larger than that at 0.1 Hz. They discussed the progression of shear strain amplitudes and energy loss during torsional fatigue tests, and estimated a convergence value of energy loss per unit cycle that was not related to the initiation and propagation of microfractures in the specimen.

The authors investigated the fatigue strength of wood under cyclic tension-torsion combined loading experimentally (Sasaki and Yamasaki 2002). The material used for the experiments was a rectangular bar of air-dried Japanese cypress. A pulsating triangular axial load of tension was applied along the longitudinal direction at 1 Hz, while the specimen was also simultaneously subjected to a twisting moment at the same phase around the longitudinal axis of the specimen, which coincided with the fiber direction of the wood. The mechanical behavior of the wood under combined stress was investigated. The obtained results of fatigue tests showed that they are affected by the combined-stress ratios and the applied stress levels. All data were located in a relatively wide band on the *S-N* plot despite the different combined-stress ratios, but the slope of the *S-N* curves decreased when the tensile stress was dominant.

Recently, there has been significant technical development of the timber structure in fields of civil engineering and construction. Understanding the mechanical behavior of wood under combined loading is required not only in the case of a uniaxial load but also in the case of torsion and axial loads acting simultaneously. Furthermore, natural materials, such as wood and bone, possess structures fulfilling the requirements of support and transport of nutrients, and wood has traditionally been regarded as a stereotypical orthotropic material similar to bone. Similarity in function and properties provides inspiration for investigating the possible use of wood as an implant material. For example, it is expected that information on the mechanical behavior of wood under combined stress is useful in the development of new composite materials such as artificial bone (Gross and Ezerietis 2003).

With these points as background, the torsion fatigue of wood under combined stress was investigated. In this study, a rectangular bar of Japanese cypress with the same dimensions as those in previous studies was used as the test piece, and a fatigue test was performed under both cyclic tension-torsion combined loading and cyclic compression-torsion combined loading. An axial force was applied along the fiber direction (along L) and torque was applied around the axis in the same direction as L. The experiment was aimed at investigating the torsion fatigue characteristic of wood under combined loading. That is, this research focused particularly on the effect of axial stress on the torsion fatigue strength of Japanese cypress.

EXPERIMENTAL METHODS

Sample preparation

The material used in this experiment was Japanese cypress (*Chamaecyparis obtusa* Endl.). The specimen was cut to have a rectangular cross-section with its major axis lying in the fiber direction. The dimensions of the specimen were 300 mm (L) × 17.5 mm (T) × 17.5 mm (R). In the central part of the specimen, a taper was attached to four planes and a portion with cross-sectional dimensions of 11.5 mm × 11.5 mm and length of more than 25 mm was prepared. The specimens were cured in the laboratory maintained at 25°C and a relative humidity of 40%, until the constant weights of specimens were achieved. The total number of specimens used in

this study was 115, as shown in Table 1. The average density and average moisture content were 440 ± 10 kg/m^3 and 7.8 ± 0.3 %, respectively.

Static tests and failure criterion

To determine static strength, uniaxial loading, pure torsion, compression-torsion and tension-torsion combined loading tests were first carried out. An electrohydraulic servo machine (EHF-ED 10/TD1-20L manufactured by Shimadzu Corporation, Kyoto) for the static loading tests was used. An axial force was applied in the fiber direction (along L) and torque was applied around an axis lying in the same direction as L. At the respective centers of a cross-grain plane (LT plane) and a straight-grain plane (LR plane), a triaxial rosette gage (KFG-3-120-D17 manufactured by Kyowa Electronic Instruments Co., Ltd., Tokyo, with gage length of 3 mm and 120 Ω) was attached. The applied axial force and torque, and the axial and rotational displacements were measured by load cells and electric displacement transducers on the testing machine itself, while the longitudinal and shear strains were also measured by strain gages on the LT and LR planes. All tests were carried out at 25°C and a relative humidity of 40%. The procedures for these static loading tests were as follows: In order to determine the static strengths in tension, compression, and torque, uniaxial loading and pure torsion tests were carried out under a controlled condition using a constant rate of displacement. The axial force was applied at a constant axial displacement rate of 0.01 mm/s and the torque at a constant rotational rate of 0.05°/s. In order to determine the failure surface, the combined loading tests were conducted by the proportional deformation loading method, in which the axial force and torque were applied simultaneously to the test specimen with their displacement rates kept constant. By changing the ratio of application rates of the axial displacement and rotation, a failure surface resulting from the combination of axial stress and shear stress at the time of failure was created. As loading was applied under a controlled condition using a constant rate of displacement, the displacement rate was set not to exceed 1.5 times the rate used in uniaxial loading and pure torsion tests so as to avoid the effect of impact forces. The number of specimens for each static test is shown in Table 1. Through these tests, the failure criterion that was used as the standard of a fatigue test was obtained as a combination of axial and shear strengths.

Shear stress was calculated by considering the anisotropy of wood, that is, when torque is applied to a wooden rectangular bar, in the long axis which coincided with the fiber direction (L), the shear stresses at the center of the LT and LR planes (τ_{LT} and τ_{LR}) can be obtained (Love 1927; Hearmon 1948, 1961; Okusa 1977; Suzuki and Okohira 1982; Yoshihara and Ohta 1993).

According to a previous study (Sasaki and Yamasaki 2002), it was proved that Hill's criterion approximately satisfied the failure condition. On the basis of Hill's criterion normalized

TABLE 1. *Number of specimens used in this experiment.*

Type of test	Group (stress state)	Symbol	Number of specimens	Remarks
Static tests	Pure tension		5	Results of the static tests
	Combined tension-torsion		14	were shown in a previous study
	Pure torsion		5	(Sasaki and Yamasaki, 2002).
	Combined compression-torsion		12	
	Pure compression		5	
Fatigue tests	Combined tension-torsion	TB	15	Two to five specimens
	Combined tension-torsion	TA	15	were used for each stress
	Pure torsion	S	18	level.
	Combined compression-torsion	CA	12	
	Combined compression-torsion	CB	14	

by each value of static strength, the combined-stress ratio for the fatigue tests was determined, as schematically shown in Fig. 1. Namely, the combined-stress ratio (β) is defined by the ratio of normalized axial stress to the normalized shear stress. Five β's, that is, combinations of axial and shear stresses (indicated as CB, CA, S, TA, and TB) were set up as shown in Table 2. These β's equally divided the semicircle of two quadrants for compression-shear and tension-shear combined-stress states into eight on the basis of the failure criterion, as shown in a previous study (Sasaki et al. 2005). Each number in Table 2 indicates the ratio of stress to pure axial or shear strength (σ_A/F_A or τ_S/F_S) and the values for each stress combination. As determined from these β's, the shear stress component was dominant in the combined-stress states CA and TA. In the CB and TB states, shear and axial stress components were almost equal.

Fatigue tests

A pulsating triangular twisting moment was applied along the longitudinal direction at 1 Hz, while the specimen was also simultaneously subjected to an axial (compression or tension) load along the longitudinal direction at the same phase. By this way, the relationship between axial stress and shear stress for a loading path is given by a straight line, as explained in a previous study (Sasaki and Yamasaki 2002). The same testing machine used for static tests, which could apply axial and torsional loads simultaneously, was used for fatigue tests. The stress level in the fatigue tests was determined as the ratio of maximum stress to ultimate stress, whose values are shown in Table 2, and six stages equivalent to 100, 90, 80, 70, 60, and 50% of these values were determined as the stress levels. For each stress level, 2 to 5 specimens were tested. The total number of specimens used in the fatigue tests was 74, as shown in Table 1. The applied axial force and torque, and axial and rotational displacements were measured using the load cells and the electric displacement transducers of the testing machine itself, while longitudinal and shear strain were also measured using strain gages on the LT and LR planes. These data were recorded simultaneously through a dynamic data logger at a 50-Hz sampling frequency. All the tests were carried out at room temperature (25°C) and at a relative humidity of 40%.

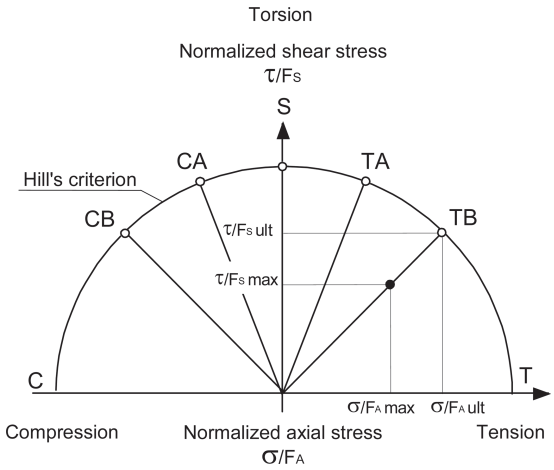

FIG. 1. Schematic of Hill's criterion and combined-stress states determined for fatigue tests.

Statistical analyses

From the results of fatigue tests, five *S-N* lines were obtained as shown in "*Fatigue life.*" To examine these data trends, three statistical analyses were performed, which were "regression analysis for the relationship between stress level and fatigue life," "analysis of covariance (ANCOVA) for the comparison of the *S-N* regression lines between five β's," and "multiple comparisons with Bonferroni adjustment to assess the individual differences in fatigue life between combined stress ratios." The acceptance criterion for statistical significance was $p < 0.05$ throughout; that is, the individual significance was set at $p < 0.05/k$ (k: number of comparisons) with Bonferroni adjustment.

The ANCOVA test included the following two tests. The first test for the homogeneity of regression was performed to examine the equality of the regression coefficient, that is, the inclination of the *S-N* line. When this equality was accepted, the second test for factorial effects was

TABLE 2. *Stress ratios and ultimate axial and shear stresses.*

Combined-stress state	Combined-stress ratio (β)*		Ultimate stress [MPa]		Remarks
	Axial	Shear	Axial (σult)	Shear (τult)	
T**	1	0	111	0.00	Pure tension
TB	0.73	0.71	81.3	16.7	Combined tension
TA	0.41	0.92	45.1	21.6	and shear
S	0	1	0.00	23.5	Pure torsion
CA	0.41	0.92	−16.7	21.6	Combined compression
CB	0.74	0.71	−30.4	16.7	and shear
C**	1	0	−41.2	0.00	Pure compression

* Each combined-stress ratio (β) indicates the ratio of stress to pure axial or pure shear strength is, σ_A/F_A or $\tau s/F_s$, respectively.
** Not demonstrated in this paper.

performed to examine the difference in stress level at the same fatigue life.

RESULTS AND DISCUSSION

Fatigue life

Figure 2 shows the *S-N* curves obtained by fatigue tests. Horizontal and vertical axes show the fatigue life (N_f) and the normalized maximum stress based on nominal stress (stress level), respectively. There exists a negative linear relationship between stress level and fatigue life on the semilogarithmic graph. Five *S-N* lines were obtained corresponding to five kinds of combined-stress states. Each straight line in the figure was obtained by the least-squares method, assuming that the life curves on the semilogarithmic plot were straight lines. All regression lines were statistically significant ($p < 0.01$), as shown in Table 3. From these, the *S-N* line of each combined-stress ratio (β) could be deduced to form one thick strap, although a variation was observed. On the basis of these *S-N* lines, we can observe that when the tension is added to pure torsion, the inclination of an *S-N* line tended to decrease as the tensile stress component increased, and the life becomes short if the stress level is high. On the other hand, when the compression is added to pure torsion, the *S-N* line generally moves to the long-life side.

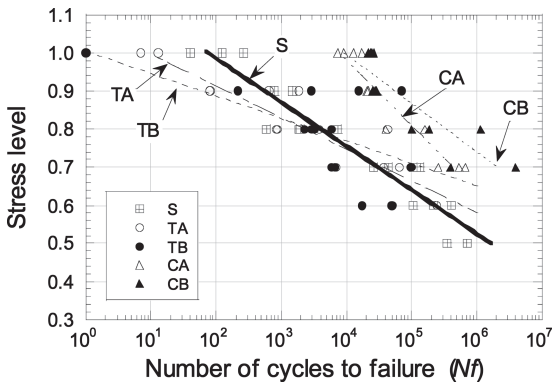

FIG. 2. Relationships between the stress level and the number of cycles to failure.

Then, the regression lines were statistically compared by ANCOVA. First, in an analytical result to the whole, it turned out that five regression lines had significant differences in both statistical tests that included ANCOVA, and the regression line of the *S-N* curve was affected by the combined-stress ratio (β): the *p*-values of "the test for homogeneity of regression" and "the test for factorial effects" were 0.0003 and 1.6×10^{-11}, respectively, which were statistically significant ($p < 0.01$). Then, the differences between two regression lines in five lines were examined individually. Tables 4 and 5 show *p*-values obtained by the two statistical tests; one was "the test for homogeneity of regression" and the other was "the test for factorial effects," respectively. In these tables, a statistical significance of $p < 0.01$ is accepted with a *p*-value of 0.0005 or less, and $p < 0.05$ with a *p*-value of 0.0025 or less, because the individual significance was adjusted by the Bonferroni method. When the homogeneity of regression, that is, the equality of inclination of the *S-N* line was examined, as shown in Table 4, a significant difference was accepted between pure-torsion S

TABLE 3. *Regression models for number of cycles to failure on fatigue strength under pulsating torsion-axial combined loading.*

Combined-stress state	Regression model (*S-N* curve)	Coefficient of determination (R^2)	*p*-value
S	$Fs = 1.2151 - 0.1149 \log (N_f)$	$R^2 = 0.90$	5.04×10^{-9}**
TA	$Fs = 1.0789 - 0.0829 \log (N_f)$	$R^2 = 0.82$	2.63×10^{-6}**
TB	$Fs = 1.0043 - 0.0587 \log (N_f)$	$R^2 = 0.48$	3.78×10^{-3}**
CA	$Fs = 1.666 - 0.1712 \log (N_f)$	$R^2 = 0.91$	1.14×10^{-6}**
CB	$Fs = 1.5048 - 0.1273 \log (N_f)$	$R^2 = 0.74$	2.83×10^{-4}**

Fs: Fatigue strength (= stress level)
N_f: Number of cycles to failure (= fatigue life)
**: Significant at 1% level

TABLE 4. *P-value obtained by the test for homogeneity of regression (pre-ANCOVA)*

Combined-stress state	TA	TB	CA	CB
S	0.0259	0.0058	0.0001**	0.0002**
TA		0.2418	0.0006*	0.0874
TB			0.0031	0.0619
CA				0.1449

* Significant at 5% level.
** Significant at 1% level.

TABLE 5. *P-value obtained by the test for factorial effects (ANCOVA).*

Combined-stress state	TA	TB	CA	CB
S	0.3448	0.8885	$(1.2 \times 10^{-9}$**)	$(1.0 \times 10^{-10}$**)
TA		0.8462	$(9.5 \times 10^{-7}$**)	6.8×10^{-8}**
TB			0.0011*	0.0002
CA				0.0270

* Significant at 5% level.
** Significant at 1% level.
() Reference values; because they were accepted as statistically significant as shown in Table 4.

and CA, in which the compression was added to pure torsion, and also between S and CB states. On the other hand, the difference between S and TA states was not significant, as well as that between S and TB states. Moreover, the inclinations of the *S-N* lines of TA and CA states were also different from each other. When the factorial effects in the *S-N* lines, that is, the differences in stress level at the same fatigue life, were examined, as shown in Table 5, the effect of axial force combined with torsion appeared more distinctly than that shown in Table 4, and the significant difference between the tension group (S, TA, and TB) and the compression group (CA and CB) was accepted. From these statistical tests that included ANCOVA, therefore, it turned out that the *S-N* line was changed by a kind of axial force slightly acting with torsion, and was much more affected by compression than tension.

As described earlier, it turned out that the *S-N* lines under five combined-stress states were different from each other. Then, how the fatigue lives would differ from each other on each stress level was analyzed. Here, the fatigue lives under CA and TA stress states were compared briefly. These are in the combined stress state with dominant torsion in which the axial load was slightly added to the torsion. Similarly, the fatigue lives of CB and TB stress states were compared. In the CB and TB states, shear and axial stresses were almost equally applied. The analytical results are shown in Fig. 3. The horizontal and vertical axes show the stress level and average fatigue life, respectively. Figure 3 shows that the fatigue lives under torsion-compression combined stress state CA are longer than those under torsion-tension TA. In addition, the difference in fatigue life between under CA and TA became considerable as the stress level increased. It is considered that a similar tendency exists under CB.

Okuyama et al. (1984) conducted fatigue tests on wood under pure tension and pure compression. Their results showed that the *S-N* lines under pure compression are located at the longer-life area. In the case of the uniaxial stress state, wood is a well-known material in the sense that it is stronger in terms of static tension than in terms of static compression; however, fatigue life is shorter under pure tension. In the case of the multiaxial stress state, on the other hand, the

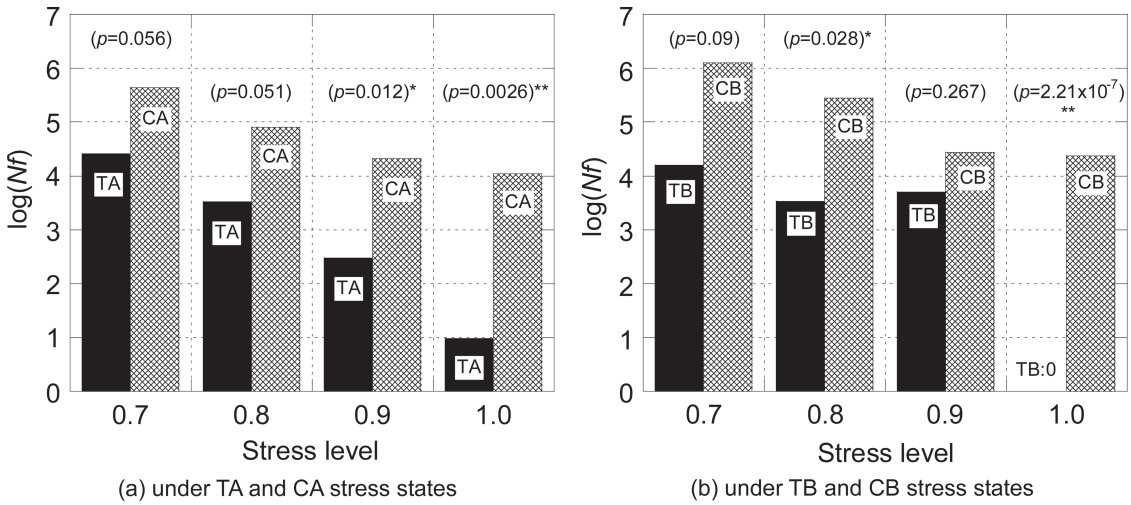

FIG. 3. Relationships between the logarithmic number of cycles to failure and the stress level.

static failure criterion indicated that the maximum shear strength under the combined stress state was located slightly on the tension side, which was almost equal to the combined stress state TA (Yamasaki and Sasaki 2004). When the dynamic loading was applied to wood, the *S-N* lines in this study under torsion and axial combined stress states were located between two *S-N* lines under pure tension and pure compression, as determined by Okuyama et al. (1984). The *S-N* lines under torsion and axial combined stress move toward the longer-life area and closer to the *S-N* line under pure compression when the compression stress becomes dominant in the combined stress state. Therefore, it is considered that fatigue life is longer under compression-torsion combined loading than under tension-torsion combined loading, in much the same way as under uniaxial stress states. This suggests that the strength properties under both uniaxial and multiaxial stress states are likely to depend on the mode of loading, that is, static or dynamic.

Torsion deformation

As described earlier, the fatigue life in the combined stress state CA, in which the compression load was slightly added to torsion, lengthened. Concerning this, the discussion is made from the viewpoint of torsion deformation.

Figure 4 shows examples of shear stress and shear strain relationships, with increasing number of loading cycles, obtained from fatigue tests. The figure on the left shows the stress-strain relationships under torsion-tension combined stress state TB, and that on the right shows those under torsion-compression stress state CB, in which the stress level is 0.9 in both stress states. The maximum shear stresses ($\tau_{max} = 0.9\tau_{ult} = 15.03$ MPa) are equally applied in both stress states during tests. Figure 4 shows the delicate change in the relationship between shear stress and shear strain with increasing number of loading cycles. Here, the maximum shear strain when the stress reached maximum was evaluated and discussed in relation to the number of loading cycles. Figure 5 shows the maximum shear strain in the vertical axis and the number of loading cycles (n) in the horizontal axis, which are standardized by fatigue life (N_f). Figure 5(a) shows the relationships under combined stress states CA, TA, and S, and Fig. 5(b), those under CB, TB, and S. The maximum shear strain in CA, TA, and S was initially almost constant with an increase in the number of loading cycles, and then increased immediately before final failure. They show almost the same tendencies, as

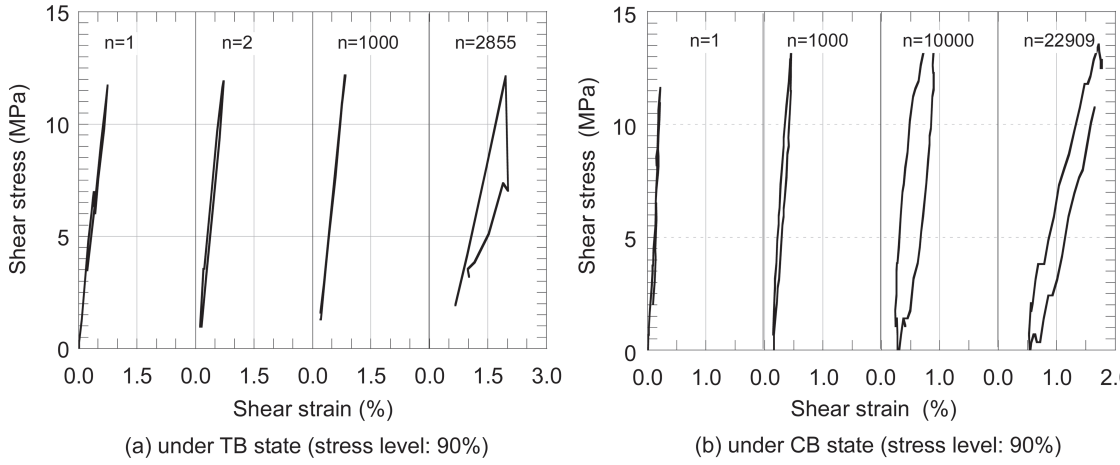

FIG. 4. Stress-strain relationships in shear under pulsating axial-torsion combined loading.

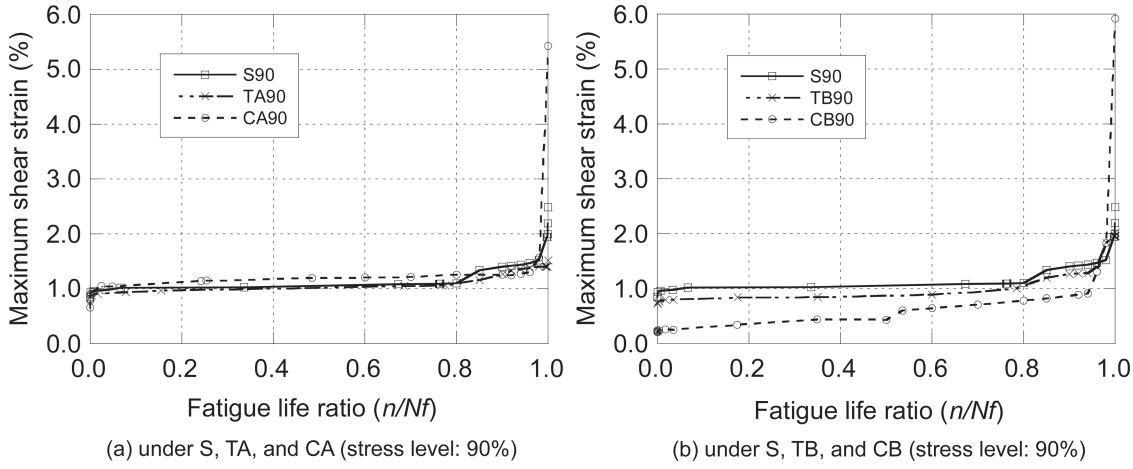

FIG. 5. Progress of the maximum shear strain under pulsating axial-torsion combined loading.

shown in Fig. 5(a). In contrast, the maximum shear strain in CB shown in Fig. 5(b), in which the output of shear strain is small, deserves attention. That is, the torsion deformation of CB kept small until the increase before final failure compared with those of TB and S.

Concerning the above result that the torsional deformation was small under stress state CB, the authors now considered this phenomenon on the basis of our past experimental result. The authors discussed the elastic properties of wood under combined static axial force and torque, and showed the relationships between shear stiffness and combined stress state in a previous study (Yamasaki and Sasaki 2003). The relationships between shear stiffness and combined static stress state showed a clear tendency under the dominantly applied axial force; that is, the shear stiffness increased as the compression was applied more dominantly, compared with the shear modulus obtained from the pure torsion test ($p < 0.01$). When a large compression was applied with torsion as in the case of CB, the warping of the specimen by torsion was considered to be restrained. Under such a condition, the specimen is subjected to two kinds of torsional moments, one is the torsional moment caused by the twisting of the specimen, and the other is the

secondary torsional moment caused by the restraint of the warping. Torsional moment as the cross-sectional force is the sum of these torsional moments, which were caused by the twisting of the specimen and the restraint of the warping (Wagner and Pretschner 1935; Komatsu 1969; Takaoka 1974). As a result, the shear strain under CB attributable to twisting is smaller than those under TB and S, as shown in Fig. 5(b).

Failure mode

Figure 6 shows examples of the failure modes obtained by the fatigue tests performed under each combined-stress ratio. These examples, at a stress level of 80%, from left to right, show compressive-shear combined stress (CB), a pure torsion (S), and tensile-shear combined stress (TB) states, respectively. When the combined-stress ratio was in the S and TA states, where the shear stress component was dominant, a crack along the fiber was observed and torsion failure was considered to be dominant, at any stress levels. However, the combined failure by torsion and tension was observed in the TB state, as shown in Fig. 6. In the TB state, where tensile and shear stresses were produced at equal levels, the failure at higher stress levels seemed to be influenced considerably by tension, and the combined failure by torsion and tension was observed. However, the failure at the stress level of 60% seemed to be influenced by torsion, and torsion failure became dominant.

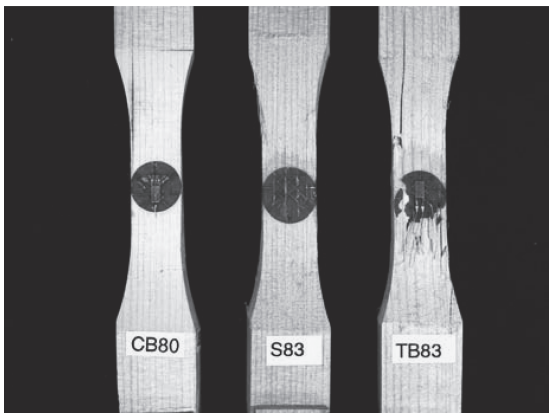

FIG. 6. Examples of failure modes by fatigue tests at a stress level of 80%. From left to right, typical failure modes under compressive-shear combined stress (CB), pure torsion (S), and tensile-shear combined-stress (TB) states are shown.

In the CA and CB states, where shear stress was applied dominantly, cracks along the fiber from torsion failure were observed, as in S and TA. In addition, almost the same destructive tendencies as shown in Fig. 6 were observed at all stress levels. The failure mode in the TB state was affected by stress level, as mentioned above. The effect of tensile stress on failure became more significant at higher stress levels, while the effect of shear stress on failure became more significant at lower stress levels. In contrast, the failure mode in compressive-shear combined stress states was not affected by the stress level.

CONCLUSIONS

When tension was added to pure torsion, the inclination of an *S-N* curve tended to decrease as the tensile stress component increased, and the life became short if the stress level was high. On the other hand, when compression was added to pure torsion, the *S-N* curve generally moved to the long-life side. The strength of a wood specimen was different between dynamic and static modes, under not only pure loading but also axial-torsion combined loading. Shear strain under compression-torsion combined loading remained small until the increase before final failure. This could be attributable to the restraint of warping of the specimen due to compression.

Results obtained in this study would be anticipated as a potential application in timber construction design under a complex stress such as a rigid-frame construction, or in the development of new composite materials such as artificial bone.

REFERENCES

ANDO, K., M. YAMASAKI, J. WATANABE, AND Y. SASAKI. 2005. Torsional fatigue properties of wood. Mokuzai Gakkaishi (J. Jpn. Wood Res. Soc.). 51:98–103.

GROSS, K. A., AND E. EZERIETIS. 2003. Juniper wood as a

possible implant material. J. Biomed. Mater. Res. 64A:672–683.

HEARMON, R. F. S. 1948. The elasticity of wood and plywood. His Majesty's Stationery Office, London. 10 pp.

———. 1961. An introduction to applied anisotropic elasticity. Oxford University Press, London. 51 pp.

KOMATSU, S. 1969. Theory and Calculation for Thin-Walled Structures. I. Sankaido, Tokyo. 218 pp.

LOVE, A. E. H. 1927. A treatise on the mathematical theory of elasticity. Dover, New York. Pp. 310–328.

OKUYAMA. T., A. ITOH, AND S. N. MARSOEM. 1984. Mechanical responses of wood to repeated loading I.—Tensile and compressive fatigue fractures. Mokuzai Gakkaishi (J. Jpn. Wood Res. Soc.). 30:791–798.

OKUSA, K. 1977. On the prismatical bar torsion of wood as elastic and plastic material with orthogonal anisotropy. Mokuzai Gakkaishi (J. Jpn. Wood Res. Soc.). 23:217–227.

OTTO, L. R., AND M. T. LONGNECKER. 2000. An introduction to statistical methods and data analysis. Duxbury Press, Massachusetts, 943 pp.

SASAKI, Y., AND M. YAMASAKI. 2002. Fatigue strength of wood under pulsating tension-torsion combined loading. Wood Fiber Sci. 34: 508–515.

———, AND ———. 2004. Effect of pulsating tension-torsion combined loading on fatigue behavior in wood. Holzforschung 58:666–672.

———, ———, AND T. SUGIMOTO. 2005. Fatigue damage in wood under pulsating multiaxial-combined loading. Wood Fiber Sci. 37:232–241.

SUZUKI, N., AND Y. OKOHIRA. 1982. On the measurement of shearing strength by means of the torsion test of wood sticks with rectangular cross section. Bull. Fac. Agr. Mie Univ. 65:41–49

TAKAOKA, N. 1974. Torsion Analysis of Structural Members. Kyoritsu Shuppan, Tokyo. Pp. 77–78.

WAGNER, H., AND W. PRETSCHNER. 1935. Verdrehung und Knickung von Offnen Profilen. Luftfahrtforshung. 11:174–180.

YAMASAKI, M. AND Y. SASAKI. 2003. Elastic properties of wood with a rectangular cross section under combined static axial force and torque J. Mater. Sci. 38:603–612.

———, AND ———. 2004. Yield behavior of wood under combined static axial force and torque Exp. Mech. 44:221–227.

YOSHIHARA, H., AND M. OHTA. 1993. Measurement of the shear moduli of wood by the torsion of a rectangular bar. Mokuzai Gakkaishi (J. Jpn. Wood Res. Soc.). 39:993–997.